Oil & Natural Gas Technology

DOE Award No.: DE-FE0013889

Quarterly Research Performance Progress Report (Period ending 03/31/2016)

THCM Coupled Model For Hydrate-Bearing Sediments: Data Analysis and Design of New Field Experiments (Marine and Permafrost Settings)

Project Period (10/1/2013 to 09/30/2016)

Submitted by:

Marcelo Sanchez Project PI

Texas A&M University
DUNS #: 847205572
College Station, TX
979-862-6604
msanchez@civil.tamu

Prepared for:
United States Department of Energy
National Energy Technology Laboratory
Submission date: 05/09/2016

Office of Fossil Energy

DISCLAIMER

ACCOMPLISHMENTS

The experimental study of hydrate bearing sediments has been hindered by the very low solubility of methane in water (lab testing), and inherent sampling difficulties associated with depressurization and thermal changes during core extraction. This situation has prompted more decisive developments in numerical modeling in order to advance the current understanding of hydrate bearing sediments, and to investigate/optimize production strategies and implications. The goals of this research is to addresses the complex thermo-hydro-chemo-mechanical THCM coupled phenomena in hydrate-bearing sediments, using a truly coupled numerical model that incorporates sound and proven constitutive relations, satisfies fundamental conservation principles. This tool will allow us to better analyze available data and to further enhance our understanding of hydrate bearing sediments in view of future field experiments and the development of production technology.

ACCOMPLISHED

The main accomplishments for this first period address Tasks 5, 6 and 7 of the original research plan, and include:

- Update of constitutive equations.
- Update of THCM-Hydrate.
- Numerical analyses.
- Incorporation of additional THCM-Hydrate code modifications.
- Production Optimization of Future Field Studies.

Training

The training of the two PhD students working in this project has continued during this period. Mr. Xuerui (Gary) Gai was hired at the start of the project and his activities have been related to the use of code "THCM-Hydrate"; which is the numerical tool under development in this project. His research has focused on the mechanical modeling of Hydrate Bearing Sediments (HBS). Mr. Mehdi Teymouri was hired at the beginning of the second year of the project. His research has focused on modeling numerical and analytical methods in hydrates research. He is also working in sand production when producing gas from methane hydrate reservoirs. Both students have progressed positively with their coursework at their respective universities.

Literature review

The literature review (Task 2) was completed in a previous period.

Update of Update of THCM-Hydrate

The update of the constitutive laws for hydrate-bearing marine sediments and HBS in the permafrost (i.e. Task 3) was completed in a previous period.

Close-form analytical solutions

The review on the main governing evolution laws, parameters, dimensionless ratios and simplifying assumptions for HBS dissociation (i.e. Task 4) was completed in the previous period.

Numerical analyses

The numerical analyses to solve field production experiments as boundary value problems have continued in this period. In page 6 one of the cases analyzed is presented. In page 18 a study related to the volume expansion and compressibility of the phases during dissociation is introduced.

Plan - Next reporting period

We will advance analytical and numerical fronts to enhance our code to solve coupled THCM problems involving with HBS, with renewed emphasis on simulating the natural processes under *in-situ* conditions and gas production.

.

Milestones for each budget period of the project are tabulated next. These milestones are selected to show progression towards project goals.

	Milestone Title Planned Date and Verification Method	Actual Completion Date	Comments
Title Related Task / Subtasks Planned Date Verification method	Complete literature review 2.0 / 2.a March 2014 Report	March 2014	Completed
Title Related Task / Subtasks Planned Date Verification method	Complete updated Constitutive Equations 2.0 / 2.b & 2.c June 2014 Report (with preliminary validation data)	July 2014	Completed
Title Related Task / Subtasks Planned Date Verification method	Validate new THCM constitutive equations 3.0 / 3.a, 3.b & 3.c September 2014 Report (with first comparisons between experimental and numerical results)	September 2014	Completed
Title Related Task / Subtasks Planned Date Verification method	Complete close-form analytical solutions 4.0 / 4.a & 4.b February 2015 Report (with analytical data)	February 2015	Completed
Title Related Task / Subtasks Planned Date Verification method	Complete numerical analyses 5.0 / 5.a, 5.b & 5.c July 2015 Report (with analytical and numerical data)	July 2016	Progressing as planned
Title Related Task / Subtasks Planned Date Verification method	Complete THCM-Hydrate code modifications 6.0 / 6.a June 2015 Report (with numerical data)	June 2016	Progressing as planned
Title Related Task / Subtasks Planned Date Verification method	Complete production optimization 7.0 / 7.a, 7.b, 7.c, 7.d & 7.e September 2015 Report (with numerical data)	September 2016	Progressing as planned

FORCASTING MAXIMUM RECOVERABLE GAS FROM HYDRATE BEARING SEDIMENTS BY DEPRESSURIZATION INDUCED DISSOCIATION

1. Introduction

Gas production from hydrate bearing sediments (*HBS*) is based on releasing the molecules of gas from lattice components of hydrate (which results in hydrate dissociation) with the aid of depressurization, heat and/or chemical stimulation. This is a complex phenomenon since hydrate dissociation comes with interrelated thermal, hydraulic, chemical and mechanical (*THCM*) processes. For example permeability coefficient will change as a result of the variation of temperature and hydrate saturation as well as volume variation. In addition mechanical strength of sediments depends on hydrate saturation while the effective stresses are affected by depressurization. Thus, coupled *THCM* analyses are inevitable for providing realistic simulation of gas production.

When solving engineering problems both, transient and steady state analyses are very relevant. Transient solutions are typically used, amongst others, to learn about gas production rate, to investigate optimal production strategies, and to perform sensitivity studies aimed at understanding the impact of material parameters (and other factors) on gas production. Steady state analyses are equally relevant because they inform about the limit (or final condition) of the problem under study. This section studies the analytical solution for the steady state condition involving fluid flow in a cylindrical geometry and accounting for the presence of two zones of different permeability coefficients. This solution can be very useful in problems encompassing *HBS* as it provides the physical limit to the zone around a well that can experience dissociation triggered by depressurization. From this solution it is possible to learn about the maximum amount of gas that can be produced from a given reservoir under this assumptions. A similar solution was presented before (Sanchez and Santamarina, 2015) but for the case of a spherical domain.

It was found that the analytical solution for radial flow is a function of four main factors, as follows: the radius of the wellbore area and imposed pressure at wellbore; pressure at the dissociation front (which depends on reservoir temperature through the methane-hydrate phase boundary); pressure at a distant boundary (equal to reservoir initial pressure); and the ratio

between the permeability coefficients of the already dissociated hydrate sediment *'k_{Sed}'* and the hydrate bearing sediments 'k_{HBS}'.

The same radial flow problem was solved using the coupled *THCM* numerical code that is being developed in this project to analyze problems involving gas *HBS*. The finite element (*FE*) computer program takes into consideration thermal and hydraulic processes in deformable sediments, and it also account for the changes in sediment properties in the presence of hydrate dissociation. It is based on a fully coupled formulation that incorporates the different phases and species existing in *HBS* (including hydrate and ice) and it has been implemented in CODE_BRIGHT (Olivella et al., 1996), an existing coupled multiphysics program for geological media.

To validate the *FE* program, the results of the analytical solution discussed above, were compared against the outputs of a numerical model replicating the same conditions. The effects of critical factors were also analyzed. The comparisons between the analytical solution and the finite element model were very satisfactory.

2. Analytical Solution – Cylindrical Flow Conditions

At steady-state conditions, the pressure distribution in radial flow is inversely proportional to the logarithm of the radial distance to the well. Therefore there is a physical limit to the zone around a well that can experience pressure-driven dissociation. A simple yet robust set of equations to estimate limits for gas production from hydrate bearing sediments using depressurization has been proposed.

Considering radial flow conditions governed by Darcy's law in a thin and confined reservoir with impermeable layers, the following equations are derived:

$$v = k\frac{dh}{dr} \tag{1}$$

$$v = \frac{q}{2\pi rH} \tag{2}$$

where v [m/Sec] is the flow velocity at any specified points, k [m/Sec] is the hydraulic conductivity of medium, h [m] is the head pressure at any specified point of reservoir (since it is a thick reservoir, the variation of head pressure due to elevation is negligible), r [m] is the radius

of any specified point from the center of wellbore area, q [m^3/Sec] defines the flow at specific any point and H [m] is the thickness of sediments. By combining these two equations and solving them in cylindrical coordinates, the flow equation could be written as:

$$\int_{r_1}^{r_2} \frac{qdr}{r} = -\int_{h_1}^{h_2} (2\pi kH)dh \tag{3}$$

The flow between two given points can be calculated as:

$$q = -\frac{2\pi kH(h_2 - h_1)}{\ln(\frac{r_2}{r_1})} \tag{4}$$

2.1. Steady State Condition

Two zones can be identified under steady state conditions when the pressure drop is kept constant and hydrates stop dissociating: the inner zone where hydrate has been depleted and the outer zone where hydrate remains stable (Figure 1). Let's define the size of the produced zone as r^* [m], and the total head pressure at a distant boundary as h_{far} [m]. The inner zone is characterized by the permeability of the sediment without hydrates *'k_{Sed}'* and the outer zone by the permeability of the hydrate bearing sediment *'k_{HBS}'*. Clearly, gas was produced from the inner zone *'$r \le r^*$'*. Therefore at steady state conditions the following equations are valid:

$$q_{Sed} = q_{HBS} \tag{5}$$

$$\frac{2\pi k_{Sed} H\left(h^* - h_w\right)}{\ln\left(\frac{r^*}{r_w}\right)} = \frac{2\pi k_{HBS} H\left(h_{far} - h^*\right)}{\ln\left(\frac{r_{far}}{r^*}\right)} \tag{6}$$

In the above equations, h^* [m] and h_w [m] are the head pressure at dissociation front and at wellbore area respectively, and r_w [m] is the radius of well. Based on the aforementioned equation, at steady state conditions, the ultimate radius *'r^*'* of the dissociated area is:

$$r^* = \left(r_w r_{far}^{\left(\frac{k_{Sed}}{k_{HBS}}\right)\left(\frac{h^* - h_w}{h_{far} - h^*}\right)} \right)^{\left(1 + \left(\frac{k_{Sed}}{k_{HBS}}\right)\left(\frac{h^* - h_w}{h_{far} - h^*}\right)\right)^{-1}} \tag{7}$$

As shown above, according to this simple yet robust analytical solution, the ultimate radius of pressure induced dissociation front in a thick and confined hydrate deposit is a function of (Figure 1): 1) the radius of the wellbore area *'r_w'* and wellbore head pressure *'h_w'*; 2) head pressure at the dissociation front *'h^*'* (which in turns depends on reservoir temperature through the methane hydrate phase boundary); 3) head pressure at a distant boundary *'h_{far}'* (equal to reservoir initial pressure); and 4) the ratio between the hydraulic conductivity of the already dissociated hydrate sediment *'k_{Sed}'* and the hydrate bearing sediments *'k_{HBS}'*.

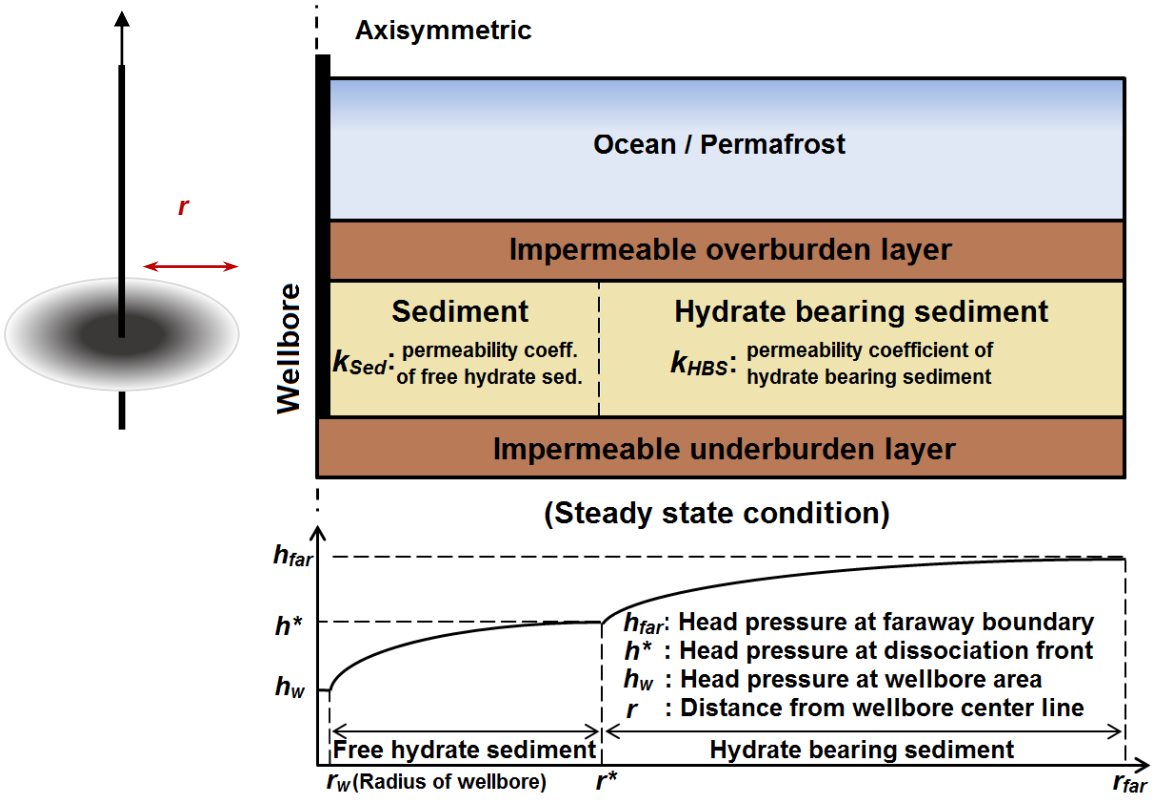

Figure 1. Two zones can be identified under steady state conditions when the pressure drop is kept constant and hydrate stops dissociating: an inner zone where hydrate has been depleted and an outer zone where hydrate remains stable.

3. Numerical Models

The aforementioned analytical solution was used to verify the coupled *THCM* numerical code for *HBS*. To solve this case, the following components were considered in the analysis: balance

equations, constitutive equations and equilibrium restrictions. A brief explanation of these equations is presented below.

3.1. Balance Equations

The mass of water per unit volume of the porous medium combines the mass of water in the liquid, hydrate and ice phases. The water flux associated to the liquid, hydrate and ice phase with respect to a fixed reference system combines Darcian flow with respect to the solid phase *'q_l'* [m/Sec] and the motion of the whole sediment with velocity **v** [m/Sec] relative to the fixed reference system. Then, the water mass balance can be expressed as:

$$\frac{\partial}{\partial t}[(\rho_l S_l + \alpha\rho_h S_h + \rho_i S_i)\phi] + \nabla.[\rho_l q_l + \rho_l S_l \phi\mathbf{v} + \alpha\rho_h S_h \phi\mathbf{v} + \rho_i S_i \phi\mathbf{v}] = f^w \tag{8}$$

where ρ [kg/m^3] represents the mass density of phases, S_β *(β=l,h,i)* indicates the phase saturation, α is the mass fraction of water in hydrate and f^w [kg/(m^{3}Sec)] stands for the external water mass supply per unit volume of the medium.

The total mass of methane per unit volume of the hydrate bearing sediment is computed by adding the mass of methane per unit volume of the gas and hydrate phases taking into consideration the volume fraction S_g and S_h, the mass fraction of methane in hydrate *'1-α'*, and the porosity of porous medium ϕ. As in the case of water balance, the flux of methane in each phase combines advective terms relative to the porous matrix and the motion of the porous medium with velocity relative to the fixed reference system:

$$\frac{\partial}{\partial t}[(\rho_g S_g + (1-\alpha)\rho_h S_h)\phi] + \nabla.[\rho_g q_g + \rho_g S_g \phi\mathbf{v} + (1-\alpha)\rho_h S_h \phi\mathbf{v}] = f^m \tag{9}$$

In this case, f^m [kg/(m^{3}Sec)] is an external supply for methane, expressed in term of mass of methane per unit volume of porous medium.

The mineral specie is only found in the solid particles. The mass balance equation follows:

$$\frac{\partial}{\partial t}[\rho_s(1-\phi)] + \nabla.[\rho_s(1-\phi)\mathbf{v}] = 0 \tag{10}$$

where ρ_s [kg/m^3] is the mass density of the mineral that make the solid particles.

3.2. Constitutive Equations

The governing equation are finally written in terms of the unknowns when constitutive equations that relate unknowns to dependent variables are substituted in the balance equations. Given the complexity of the problem, simple yet robust constitutive laws are selected for this simulation.

The advective fluxes of the liquid and the gas phases $\mathbf{q}_\ell$ and $\mathbf{q}_g$ [m/s] are computed using the generalized Darcy's law (Gens and Olivella, 2001):

$$\mathbf{q}_\alpha = -\mathbf{K}_\alpha \left(\nabla P_\alpha - \rho_\alpha \mathbf{g}\right) \qquad \alpha = \ell, g \tag{11}$$

where P_α [N/m2] is the phase pressure, and the vector **g** is the scalar gravity g=9.8 m/s^2 times the vector $[0,0,1]^T$. The tensor $\mathbf{K}_\alpha$ [m^4/(Ns)] captures the medium permeability for the α-phase; if the medium is isotropic, $\mathbf{K}_\alpha$ is the scalar permeability K_α times the identity matrix. The permeability K_α depends on the intrinsic permeability k [m^2] of the medium, the dynamic viscosity of the α-phase μ_α [N.s/m^2] and the relative permeability $k_{r\alpha}$ [ ]:

$$\mathbf{K}_\alpha = \mathbf{k}\frac{k_{r\alpha}}{\mu_\alpha} \tag{12}$$

The viscosity of the liquid μ_ℓ [Pa.s] phase varies with temperature T [°K] (i.e. Olivella, 1995):

$$\mu_\ell = 2.1\cdot 10^{-6} \exp\left(\frac{1808.5}{T}\right) \tag{13}$$

While the viscosity of gases is often assumed independent of pressure, experimental data in the wide pressure range of interest shows otherwise. Published data in Younglove and Ely (1987) are fitted to develop a pressure and temperature dependent expression for the viscosity of methane gas (fitted range: 270°K<T<290°K and 0.1MPa<P_g<40MPa).

$$\mu_g = 10.3\cdot 10^{-6}\left[1 + 0.053\frac{P_g}{\left(\frac{280}{T}\right)^3}\right] \tag{14}$$

To reproduce the conditions of the analytical solution analyzed in this report, no changes in porosity induced by mechanical effects are considered, in this case the changes in *HBS* permeability induced by hydrate dissociation can be written as

$$k_{HBS} = k_{sed}\left(1 - S_h\right)^N \tag{15}$$

where N [-] is related to hydrate deposit morphology.

The relative permeabilities for liquid $k_{r\ell}$ and gas k_{rg} increase as the degree of saturation of each phase increases with respect to the mobile phase saturation $S_\ell+S_g$. A single parameter power function properly reproduces experimental data

$$k_{r\ell} = \left(\frac{S_\ell}{S_\ell + S_g} \right)^a = \left(S_\ell^* \right)^a \tag{16}$$

$$k_{rg} = \left(1 - \frac{S_\ell}{S_\ell + S_g} \right)^b = \left(1 - S_\ell^* \right)^b \tag{17}$$

where = $S_\ell/(S_\ell+S_g)$ is the effective liquid saturation in the hydrate bearing sediment. The hydraulic conductivity of reservoir deposit is highly affected by hydrate concentration and hydrate morphology.

The interfacial tension between liquid and gas sustains the difference between the liquid and gas pressures P_ℓ and P_g. The capillary pressure and the effective liquid saturation S_ℓ^* are related (van Genuchten, 1978):

$$S_\ell^* = \frac{S_\ell}{S_\ell + S_g} = \left[1 + \left(\frac{P_c}{P_o} \right)^{\frac{1}{1-\lambda}} \right]^{-\lambda} \tag{18}$$

where P_o and λ are model parameters.

3.3. Phase Boundaries

Pressure and temperature defined the phase boundary for methane hydrate and ice. The selected expression for the phase boundary of methane follows the format in Sloan and Koh (2008), but it is adjusted to stratify values computed using the *HWHYD software*.

$$P_{eq} = e^{\left(40.234 - \frac{8860}{T_{eq}[^\circ K]}\right)} \tag{19}$$

where P_{eq} is the equilibrium pressure [kPa]. Local equilibrium conditions are attained much faster than the duration of the global process in most *THCM* problems.

3.4. Simulation

Several models were prepared based on various reservoir initial conditions and also different production strategies by imposing a variety of possible pressures at the wellbore to verify the code performance when compared against the results from the analytical solution. These analyses also allowed studying the effect of crucial parameters and factors related to the problem of hydrate dissociation induced by depressurization. Table 1, presents the initial reservoir conditions and also the imposed pressure at the wellbore for the cases studied in this report.

Table 1. Cases considered in the analysis

Case	h_{far} (m)	h_w (m)	T ($^\circ$C)	$\frac{h^* - h_w}{h_{far} - h^*}$
A	1020	306	12	7.14
B	1224	306	12	2.14
C	1224	510	12	1.44
D	1224	306	10	0.91
E	1224	306	8	0.47

An intrinsic permeability coefficient for hydrate bearing sediments k_{HBS}=1x10^{-12} m^2 was considered in all the models (Eq. 15). A hydrate saturation S_h=0.5 was adopted. The different ratios between already dissociated hydrate sediment permeability coefficient (k_{Sed}) and k_{HBS} were obtained by adopting different values of the hydrate morphology coefficients N.

A long (L=1.20km) and thin (h=0.40m) domain was adopted in the analyses. A 2D axisymmetric geometry was modeled based on a single vertical well producing from a cylindrical section with a very fine grids. Mesh discretization along the radial direction was not uniform, increasing logarithmically from 0.12m at r_w to 0.80m at r_{max}. The final discretization consists of 5008 nodes and 2503 elements. This high degree of refinement provided the level of detail required to capture crucial processes near the wellbore and the entire *HBS* layer.

Table 2. Model parameters used in numerical simulation

Parameter	Value
Initial saturation	S_h=0.50, S_l=0.50, S_g=0.00
Intrinsic permeability in *HBS*	k_{HBS}=1x10^{-12} m^2 (Isotropic: $k_x = k_y = k_z$)
Porosity of *HBS*	ϕ=0.40
Capillary pressure model	P_o=100 kPa; λ=0.5
Liquid relative permeability model	$a = 1$
Gas relative permeability model	$b = 1$

To reach the steady state condition, a long term depressurization was considered in the numerical analyses. In some occasions, the steady state condition were not fully achieved (even for the very long time duration performed analyses). In these cases, the final conditions were not very far from the steady state ones. In fact, in practically all the cases analyzed, the analytical solution predicted a little bit further dissociation front than the *FE* solution. Therefore, it appears that if the models would run for longer times, both results could match even better. In all the cases, the radii of wellbore area was r_w=0.1m, and a very long length of the reservoir is modelled to have a realistic distant (fix) boundary condition. It is also assumed that the rate of heat conductivity is high enough to compensate the temperature reduction due to the endothermic behavior of hydrate dissociation by reaching the steady state condition. Therefore the head of pressure at dissociation front *'h*'* is derived from methane hydrate phase boundary diagram for a given reservoir initial temperature.

Figure 2 presents the results of the discussed analytical solution (dash lines) for the different cases listed in Table 1, showing the interplay between the relative sediment permeability coefficients *'k_{Sed}/k_{HBS}'* and the relative pressure dissociation *'$(h^* - h_w)/(h_{far} - h^*)$'*. As shown, the numerical results (solid line) are very satisfactory when compared against the analytic ones for the variety range of conditions analyzed.

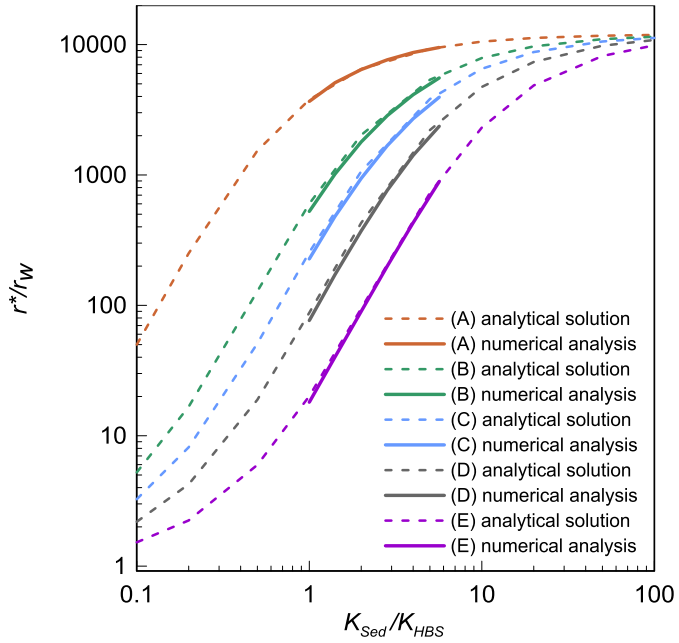

Figure 2. Results obtained with the analytical solution and numerical models for the different cases listed in Table 1.

Moreover, the effect of some relevant parameters related to methane production from gas-hydrate induced by depressurization is illustrated in Fig.2. As expected, it is predicted that the dissociation front will be farthest from the well in those cases in which the permeability coefficient increases more with hydrate dissociation. This implies that the degree of permeability enhancement by dissociation (which depends on hydrate morphology) plays an essential role in the depressurization propagation in *HBS*. When comparing *Cases A*, *B* and *C* for the same initial and wellbore pressure, it shows that the more gas hydrate is released from warmer reservoir. It is also observed that *Cases A* and *C* have the same hydraulic gradient between wellbore area and distant boundary, as well as, the same initial temperature but with different initial pressure. The lower initial pressure of reservoir, the higher amount of produced gas.

4. Discussion

A closed-form analytical solution was developed to analyze the steady state conditions related to gas production from gas hydrate bearing sediments for the case of radial flow in a cylindrical domain. This analytical solution was then adopted to validate the *THCM* coupled computer code that is being developed in this project. The performance of the proposed framework was very satisfactory when comparing the analytical and numerical model results.

VOLUME EXPANSION DURING HYDRATE DISSOCIATION

1. Introduction

Xu and Germanovich (2006) quantified the excess pore pressure resulting from gas hydrate dissociation in marine sediments due to continuous sedimentation, tectonic uplift, sea level fall, heating or inhibitor injection. Amongst others, they found the excess pore pressure as a trigger of submarine landslides in shallow water environments. In this report, some of the concepts discussed by Xu and Germanovich (2006) were used to study the volume expansion during hydrate dissociation.

Gas hydrates are solid compounds consisting of water molecules clustered around low molecular weight gas molecules. According to mass balance equations, the mass of this solid compound should be equal to the summation mass of released water and gas molecules after dissociation:

$$m_h = m_l + m_g \tag{1}$$

Hydrate molecular structure is indicated by hydrate number. Therefore, the water mass fraction in hydrate solid compound *'α'* could be derived as,

$$\alpha = \frac{m_l}{m_h} = \frac{X}{(0.89 + X)} \tag{2}$$

Note that for the case of methane-hydrate: $X=5.75$ and $\alpha=0.866$

It can be concluded that the following equations are valid for the mass fraction of water and gas molecules composing a molecule of hydrate.

$$m_l = \alpha\, m_h \tag{3}$$

$$m_g = (1-\alpha)\, m_h \tag{4}$$

The variation of void volume due to dissociation is the summation of changing volume of hydrate, gas and liquid phases. The amount of volume expansion could be derived:

$$\frac{dV_V}{V_V} = \frac{dV_l + dV_g + dV_h}{V_V} = \frac{\left(\alpha\left(\frac{\rho_h}{\rho_l}\right) + (1-\alpha)\left(\frac{\rho_h}{\rho_g}\right) - 1\right) dV_h}{V_V} = R_V dS_h \tag{5}$$

where dS_h represents de reduction in hydrate saturation because of dissociation.

$$R_V = \alpha\left(\frac{\rho_h}{\rho_l}\right) + (1-\alpha)\left(\frac{\rho_h}{\rho_g}\right) - 1 \tag{6}$$

where R_V is the factor of volume expansion resulting from the gas hydrate dissociation, and R_v is the increment of hydrate dissociation. The minus sign for hydrate volume indicates the consumption of hydrate due to dissociation while the gas and water are released. As shown in the equations above, the factor of volume expansion inherently depends on molecular structure of hydrate *'α'* and also is a function of gas, liquid and hydrate densities. Gas and liquid densities highly depends on pressure P [MPa] and temperature T [°C], while the dependency of solid hydrate density ($\rho_h = 900 \text{kg/m}^3$) on variation of pressure and temperature is negligible.

$$\rho_l = \rho_{l_0}\left(1+\frac{P}{\beta_l}\right)\left(1-\beta_{T_l}\left[\frac{(T+273.15)-277}{5.6}\right]^2\right) \tag{7}$$

where $\rho_{l_0} = 999.8\,[\text{kg/m}^3]$, $\beta_l = 2000\,[\text{MPa}]$ and $\beta_{T_l} = 0.0002 \circ K^{-1}$.

$$\rho_g = \frac{M_m.P}{R(T+273.15)}\left[1176 + 12.7\left(\frac{P}{P_{ref}}\right) - 0.45\left(\frac{P}{P_{ref}}\right)^2\right] \tag{8}$$

where M_m=16.042 g/mole; R=8.314 J/(mol°K), and P_{ref}=1[MPa]

1.1. Factor of Volume Expansion

The factor of volume expansion *'R_V'* changes considerably through methane-hydrate phase boundary, since it is a function of liquid and gas densities which are highly dependent on pressure and temperature. Figure 3 illustrates the variation of R_V through methane-hydrate phase boundary. As shown, although the rate of volume expansion is much higher for the case of cold reservoir (permafrost region) and lower for warm reservoir.

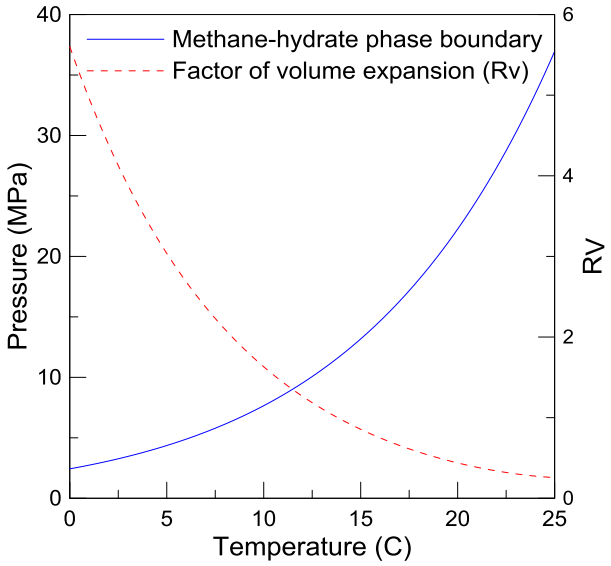

Figure 3. Factor of volume expansion variation through methane-hydrate phase boundary

1.2. Excess Pore Pressure

The volume expansion that takes place during hydrate dissociation may induce some of the following effects: i) compression of the liquid and/or gas phases (mainly associated with undrained and rigid skeleton conditions); ii) advective fluxes of gas and liquid phases (triggered by gradient of phases pressures under drained conditions); iii) sediment deformation (related to changes in effective stresses in deformable media).

As for the compression of the liquid and gas phases, it can be estimated from the excess pore pressure generated during dissociation. Considering a rigid and undrained sediment, the increment of the excess pore pressure 'P_{ex}' can be estimated as a function of the hydrate dissociation; R_v; and the equivalent volume compressibility of void phases (K_{eq}):

$$P_{ex} = \int_0^{\Delta S_h} \frac{R_V}{K_{eq}} dS_h \tag{9}$$

The compressibility coefficients of gas and liquid phases, *'K_g'* and *'K_l'* respectively, through methane-hydrate can be calculated from the following expressions:

$$K_g = \frac{\partial \rho_g}{\partial P} + \frac{\partial \rho_g}{\partial T}\frac{dT_{eq}}{dP} \tag{10}$$

$$K_g = \left[\frac{M_m}{R(T+273.15)}\right] \left[\left(1176+25.4P-1.35P^2\right)-\frac{P}{(T+273.15)}\left(1176+12.7P-0.45P^2\right)\left(\frac{8860}{\left(P\times10^3\right)\left(40.234-\ln\left(P\times10^3\right)\right)^2}\right)\right] \quad (11)$$

$$K_l = \frac{\partial\rho_l}{\partial P}+\frac{\partial\rho_l}{\partial T}\frac{dT_{eq}}{dP} \quad (12)$$

$$K_l = \left(\frac{\rho_{l_0}}{\beta_l}\right)\left(1-\beta_{T_l}\right)\left[\frac{(T+273.15)-277}{5.6}\right]^2 + \left[\rho_{l_0}\left(1+\frac{P}{\beta_l}\right)\left(-\beta_{T_l}\right)\left(\frac{1}{5.6}\right)^2(2T-554)\left(\frac{8860}{\left(\mathrm{P}\times10^3\right)\left(40.234-\ln\left(\mathrm{P}\times10^3\right)\right)^2}\right)\right] \quad (13)$$

The equivalent volume compressibility factor *'K_{eq}'* can be calculated as:

$$K_{eq} = \frac{K_g S_g + K_l S_l}{S_g + S_l} \quad (14)$$

Based on the equations above, the updated hydrate, liquid and gas saturations (S_h^u, S_l^u and S_g^u, respectively) can be written in terms of the current hydrate, liquid and gas saturations (S_h, S_l and S_g, respectively), compressibility coefficients and saturations, as follows:

$$S_h^u = S_h - dS_h \quad (15)$$

$$S_l^u = \left(S_l + \alpha\frac{\rho_h}{\rho_l}dS_h\right)\left(1-\frac{K_l\left(R_V dS_h\right)}{K_{eq}\left(S_l+S_g\right)}\right) \quad (16)$$

$$S_g^u = \left(S_g + (1-\alpha)\frac{\rho_h}{\rho_g}dS_h\right)\left(1-\frac{K_g\left(R_V dS_h\right)}{K_{eq}\left(S_l+S_g\right)}\right) \quad (17)$$

REFERENCES

Gens A., and Olivella S. (2001). "THM phenomena in saturated and unsaturated porous media." *Revue française de génie civil*, 5(6), 693-717.

Olivella S. (1995). "Non-isothermal multiphase flow of brine and gas through saline media". *Phd Thesis*, Geotechnical Engineering Department, Technical University of Catalunya, Spain.

Olivella S., Gens A., Carrera J. and Alonso, E.E. (1996). "Numerical formulation for a simulator (CODE-BRIGHT) for the coupled analysis of saline media". *Engineering Computations*; 13/7:87-112.

Sanchez M., Santamarina JC. (2015). "THCM Coupled Model For Hydrate-Bearing Sediments: Data Analysis and Design of New Field Experiments (Marine and Permafrost Settings)". *DOE Quarterly Research Performance Progress Report* (Period ending 12/31/2014).

Sloan E. D. and Koh C. A. (2008). *Clathrate hydrates of natural gases*, CRC

van Genuchten R. (1978). "Calculating the unsaturated hydraulic permeability conductivity with a new closed-form analytical model". *Water Resource Researc*, 37(11), pp. 21-28

Younglove B., and Ely J. (1987). "Thermophysical Properties of Fluids II Methane, Ethane, Propane, Isobutane, and Normal Butane". *Journal of Physical and Chemical Reference Data* 16 (4): 577

Xu W., Germanovich LN. (2006). "Excess pore pressure resulting from methane hydrate dissociation in marine sediments: A theoretical approach". *Journal of Geophysical Research*, Vol. 111, B01104.

PRODUCTS

Publications – Presentations:

- A journal paper has been accepted for publication in Environmental Geotechnics. Title: "Mechanical Modeling of Gas Hydrate Bearing Sediments Using an Elasto-Plastic Framework". Authors: Xuerui Gai, and M. Sanchez.
- A journal paper has been accepted McCartney J., Sánchez M., Tomac I. (2016). "Energy Geotechnics: Advances in Subsurface Energy Recovery, Storage, Exchange, and Waste Management". Computers and Geotechnics. doi:10.1016/j.compgeo.2016.01.002.
- A journal paper was submitted for publication. Title: "A Constitutive Mechanical Model for Gas Hydrate Bearing Sediments Incorporating Inelastic Mechanisms". Authors: M. Sanchez, Xuerui Gai, and J.Carlos Santamarina.
- Sánchez M., Santamarina J.C., Gai X, Teymouri M., and Shastri A. (2016). "Coupled Thermo-Hydro-Chemo-Mechanical (THCM) Models for Hydrate-Bearing Sediments". *Fire in the Ice*, Vol 16(1) 12-17.

Website: Publications (for academic purposes only) and key presentations are included in: http://engineering.tamu.edu/civil/people/msanchez

Technologies or techniques: None at this point.

Inventions, patent applications, and/or licenses: None at this point.

Other products: None at this point.

PARTICIPANTS

Research Team: The current team is shown next.

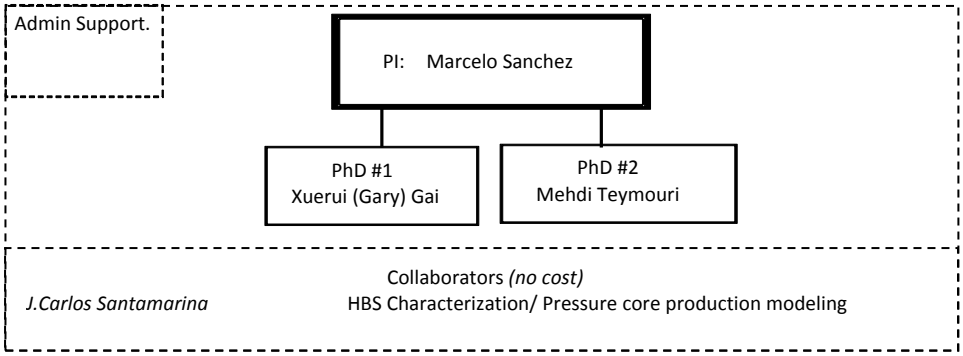

IMPACT

- We can already highlight the computational platform extensively validated in a wide range of coupled thermo-hydro-chemo-mechanical coupled problems (CB_Hydrate).

CHANGES/PROBLEMS:

None so far.

SPECIAL REPORTING REQUIREMENTS:

Nothing to report

BUDGETARY INFORMATION:

	Budget Period 1								Budget Period 2								Budget Period 3			
	Q1		Q2		Q3		Q4		Q1		Q2		Q3		Q4		Q1		Q2	
	Enter date range		Enter date range		Enter date range		Enter date range		Enter date range		Enter date range		Enter date range		Enter date range		Enter date range		Enter date range	
Baseline Reporting Quarter	10/1/13-12/31/13		01/01/14-03/31/14		04/01/14-06/30/14		07/01/14-9/30/14		10/1/14-12/31/2014		01/01/15-03/31/15		04/01/15-06/30/15		07/01/15-9/30/15		10/1/15-12/31/2015		01/01/16-03/31/16	
	Q1	Cumulative Total	Q2	Cumulative Total	Q3	Cumulative Total	Q4	Cumulative Total	Q1	Cumulative Total	Q2	Cumulative Total	Q3	Cumulative Total	Q4	Cumulative Total	Q1	Cumulative Total	Q2	Cumulative Total
Baseline Cost Plan	$ 40,500.00	$ 40,500.00	$ 40,500.00	$ 81,000.00	$ 40,500.00	$ 121,500.00	$ 92,180.00	$ 213,680.00	$ 27,600.00	$ 241,280.00	$ 27,600.00	$ 268,880.00	$ 27,600.00	$ 296,480.00	$ 92,080.00	$ 388,560.00	$ -	$ 388,560.00	$ -	$ 388,560.00
Federal Share	$ 40,500.00	$ 40,500.00	$ 40,500.00	$ 81,000.00	$ 40,500.00	$ 121,500.00	$ 92,180.00	$ 213,680.00	$ 27,600.00	$ 241,280.00	$ 27,600.00	$ 268,880.00	$ 27,600.00	$ 296,480.00	$ 92,080.00	$ 388,560.00	$ -	$ 388,560.00	$ -	$ 388,560.00
Non-Federal Share	$ 11,223.00	$ 11,223.00	$ 11,223.00	$ 22,446.00	$ 11,223.00	$ 33,669.00	$ 11,223.00	$ 44,892.00	$ 11,223.00	$ 56,115.00	$ 11,223.00	$ 67,338.00	$ 11,223.00	$ 78,561.00	$ 11,223.00	$ 89,784.00	$ -	$ 89,784.00		$ 89,784.00
Total Planned	$ 51,723.00	$ 51,723.00	$ 51,723.00	$ 103,446.00	$ 51,723.00	$ 155,169.00	$ 103,403.00	$ 258,572.00	$ 38,823.00	$ 297,395.00	$ 38,823.00	$ 336,218.00	$ 38,823.00	$ 375,041.00	$ 103,303.00	$ 388,560.00	$ -	$ 388,560.00	$ -	$ 378,732.88
Actual Incurred Costs	$ 5,301.83	$ 5,301.83	$ 13,764.34	$ 19,066.17	$ 33,827.48	$ 52,893.65	$ 51,567.77	$ 104,461.42	$ 80,352.17	$ 184,813.59	$ 24,626.18	$ 209,439.77	$ 19,260.19	$ 228,699.96	$ 29,858.73	$ 258,558.69	$ 13,074.57	$ 271,633.26	$ 23,720.88	$ 295,354.14
Federal Share	$ 3,335.02	$ 3,335.02	$ 9,848.68	$ 13,183.70	$ 10,170.37	$ 23,354.07	$ 58,205.62	$ 81,559.69	$ 92,208.79	$ 173,768.48	$ 31,359.66	$ 205,128.14	$ 19,260.19	$ 224,388.33	$ 29,812.17	$ 349,425.73	$ 4,088.61	$ 353,514.34		$ 83,378.74
Non-Federal Share	$ 5,182.96	$ 5,182.96	$ 20,751.77	$ 25,934.73	$ 20,743.19	$ 46,677.92	$ 29,262.19	$ 75,940.11	$ -	$ 75,940.11	$ -	$ 75,940.11	$ 8,833.66	$ 84,773.77	$ -	$ 84,773.77	$ -	$ 84,773.77	$ -	$ 84,773.77
Total Incurred costs	$ 8,517.98	$ 8,517.98	$ 30,600.45	$ 39,118.43	$ 30,913.56	$ 70,031.99	$ 87,467.81	$ 157,499.80	$ 92,208.79	$ 249,708.59	$ 31,359.66	$ 281,068.25	$ 28,093.85	$ 309,162.10	$ 29,812.17	$ 434,199.50	$ 8,985.96	$ 271,633.26	$ 23,360.37	$ 294,993.63
Varience	$ 43,205.02	$ 43,205.02	$ 21,122.55	$ 64,327.57	$ 20,809.44	$ 85,137.01	$ 15,935.19	$ 101,072.20	$ (53,385.79)	$ 47,686.41	$ 38,823.00	$ 55,149.75	$ 10,729.15	$ 65,878.90	$ 73,490.83	$ (45,639.50)	$ (8,985.96)	$ 116,926.74	$ (23,360.37)	$ 83,739.25
Federal Share	$ (1,966.81)	$ (1,966.81)	$ (3,915.66)	$ (5,882.47)	$ (23,657.11)	$ (29,539.58)	$ 6,637.85	$ (22,901.73)	$ 11,856.62	$ (11,045.11)	$ 6,733.48	$ (4,311.63)	$ -	$ (4,311.63)	$ 4,358.19	$ 46.56	$ 4,358.19	$ 4,404.75	$ 4,854.89	$ 9,259.64
Non-Federal Share	$ 6,040.04	$ 6,040.04	$ (9,528.77)	$ (3,488.73)	$ (9,520.19)	$ (13,008.92)	$ (40,485.19)	$ (53,494.11)	$ 11,223.00	$ (42,271.11)	$ 6,733.48	$ (35,537.63)	$ 2,389.34	$ (33,148.29)	$ 11,223.00	$ (21,925.29)	$ -	$ (21,925.29)	$ -	$ (21,925.29)
Total Varience	$ 4,073.23	$ 4,073.23	$ (13,444.43)	$ (9,371.20)	$ (33,177.30)	$ (42,548.50)	$ (33,847.34)	$ (76,395.84)	$ 23,079.62	$ (53,316.22)	$ 13,466.96	$ (39,849.26)	$ 2,389.34	$ (37,459.92)	$ 15,581.19	$ (21,878.73)	$ 4,358.19	$ (17,520.54)	$ 4,854.89	$ (12,665.65)

National Energy Technology Laboratory

626 Cochrans Mill Road
P.O. Box 10940
Pittsburgh, PA 15236-0940

3610 Collins Ferry Road
P.O. Box 880
Morgantown, WV 26507-0880

13131 Dairy Ashford Road, Suite 225
Sugar Land, TX 77478

1450 Queen Avenue SW
Albany, OR 97321-2198

Arctic Energy Office
420 L Street, Suite 305
Anchorage, AK 99501

Visit the NETL website at:
www.netl.doe.gov

Customer Service Line:
1-800-553-7681